JVSTA
JOURNAL OF VACUUM SCIENCE AND TECHNOLOGY A

Electronbeam controlled radio frequency discharges for plasma processing

Mark J. Kushner, Wenli Z. Collison, and David N. Ruzic

Citation: J. Vac. Sci. Technol. A **14**, 2094 (1996); doi: 10.1116/1.580086
View online: http://dx.doi.org/10.1116/1.580086
View Table of Contents: http://avspublications.org/resource/1/JVTAD6/v14/i4
Published by the AVS: Science & Technology of Materials, Interfaces, and Processing

Related Articles

Atomic-scale silicon etching control using pulsed Cl2 plasma
J. Vac. Sci. Technol. B 31, 011201 (2013)

Low-pressure inductively coupled plasma etching of benzocyclobutene with SF6/O2 plasma chemistry
J. Vac. Sci. Technol. B 30, 06FF06 (2012)

Reaction mechanisms of oxygen plasma interaction with organosilicate low-k materials containing organic crosslinking groups
J. Vac. Sci. Technol. A 30, 061302 (2012)

Inductively coupled plasma deep etching of InP/InGaAsP in Cl2/CH4/H2 based chemistries with the electrode at 20°C
J. Vac. Sci. Technol. B 30, 051208 (2012)

Angular dependences of SiO2 etch rates in C4F6/O2/Ar and C4F6/CH2F2/O2/Ar plasmas
J. Vac. Sci. Technol. A 30, 051301 (2012)

Additional information on J. Vac. Sci. Technol. A

Journal Homepage: http://avspublications.org/jvsta
Journal Information: http://avspublications.org/jvsta/about/about_the_journal
Top downloads: http://avspublications.org/jvsta/top_20_most_downloaded
Information for Authors: http://avspublications.org/jvsta/authors/information_for_contributors

ADVERTISEMENT

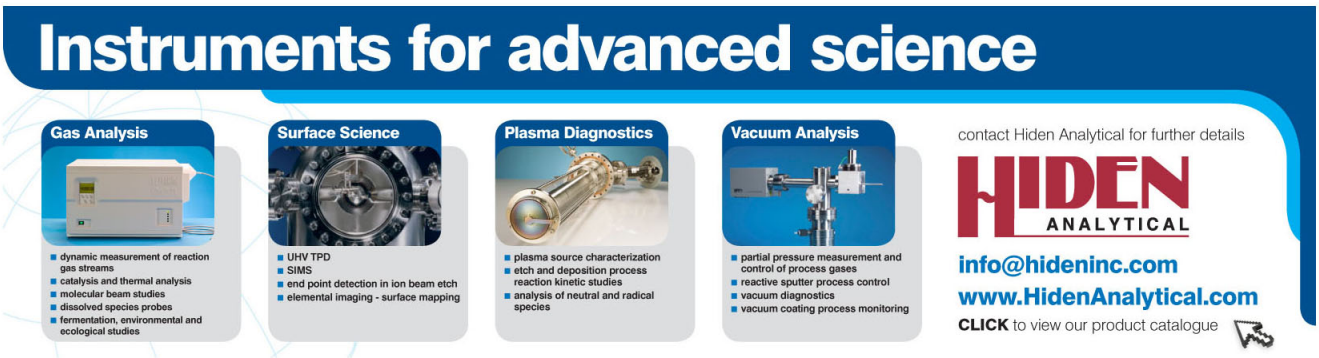

Downloaded 23 Dec 2012 to 192.17.144.173. Redistribution subject to AVS license or copyright; see http://avspublications.org/jvsta/about/rights_and_permissions

Electron-beam controlled radio frequency discharges for plasma processing

Mark J. Kushner,[a] Wenli Z. Collison,[b] and David N. Ruzic[c]
Department of Electrical and Computer Engineering, University of Illinois, 1406 West Green Street, Urbana, Illinois 61801

(Received 17 November 1995; accepted 13 March 1996)

During plasma etching and deposition of semiconductor materials, it is desirable to have separate control over the magnitude and energy of the ion flux onto the substrate. This control is difficult to achieve in reactive ion etching discharges since the radio frequency (rf) voltage applied to the substrate both generates the ions and accelerates the ions into the substrate. High plasma density devices such as electron cyclotron resonance and inductively coupled plasma reactors achieve this control by having separate power sources for ionization and ion acceleration. In this article, we present results from a computational study of an electron beam controlled rf discharge in which the production and acceleration of ions are similarly separately controlled. Ionization is dominantly produced by injection of an electron beam into the reactor. Ion acceleration is determined by a separate rf bias applied to the substrate. The limits of e-beam voltage, current, and rf bias voltage for which this separate control can be achieved will be discussed. © *1996 American Vacuum Society.*

I. INTRODUCTION

During plasma materials processing, such as the etching of semiconductors for microelectronics fabrication, it is desirable to have maximum control over the composition and energy of the reactive fluxes incident on the substrate.[1] In parallel plate radio frequency (rf) discharges, as used for reactive ion etching (RIE), this control is difficult to achieve. In these devices, the rf voltage applied to the substrate provides both the power for ionizing and dissociating the feedstock gases, and for accelerating ions into the substrate. Independent control of the magnitude, composition and energy of the ion flux onto the wafer is generally not possible. To address this difficulty, plasma sources have been developed with separate power supplies whose respective purposes are to generate and accelerate ions into the substrate. For example, in electron cyclotron resonance (ECR) discharges, the applied microwave electric field dominantly dissociates and ionizes the feedstock gases, while ions are accelerated into the wafer by a separately applied rf bias on the substrate.[2–4] The high plasma density ($>10^{11}$ cm^{-3}) in these devices produces a thin sheath; and, as a result, there is little electron heating by the rf bias to contribute to bulk ionization. A similar strategy is followed by inductively coupled plasma (ICP) etching reactors.[5–9] In these devices, power deposition from the inductively coupled electric field dominantly dissociates and ionizes the gas while a separate rf bias is applied to the substrate to accelerate ions.

In a previous publication, the concept of an electron beam controlled rf discharge (EBCRF) for plasma etching of semiconductors was introduced.[10] In the EBCRF discharge, an externally applied low voltage (1–3 kV) electron beam is injected into a low pressure rf discharge (10 s mTorr) [see Fig. 1(a)]. The intent of the EBCRF discharge is to dominantly control the dissociation and ionization of the gas, and hence the magnitude of reactive fluxes to the substrate by the electron beam. The energy of the ion flux onto the substrate is controlled by a separate rf bias. These goals are met by carefully selecting the voltage of the e-beam and the gas pressure together which determine the stopping distance of the e-beam. Once these quantities are optimized to match the stopping distance of the e-beam to the reactor dimensions, the current of the e-beam then determines the amount of excitation and ionization by the e-beam.

Additional control over the composition of the reactive flux to the substrate may also be achieved by positioning the e-beam. For example, in the experimental geometry shown in Fig. 1(a),[10] the e-beam was configured as a current sheet by masking the e-beam with the sputter shield. The height of the current sheet above the substrate can be adjusted. By doing so, one can control the location above the wafer where ions or radicals are dominantly produced. For example, ions or radicals which are generated close to the wafer will likely strike the surface without undergoing identity changing collisions such as charge exchange. If, however, one desires to change the primary ion from that produced by the beam to another ion by charge exchange collisions, one can raise the current sheet to a height which is many mean free paths from the substrate for this reaction. For example, in the Ar/Cl_2 system, the mean free path for charge exchange of Ar^+ with Cl_2 at 30 mTorr is $\simeq$1 cm. A current sheet located many cm above the substrate will produce an ion flux to the wafer which is depleted of Ar^+ due to this charge exchange process.

The application of EBCRF discharges to plasma materials processing does have some limitations. Since a dc (pulsed or otherwise) current is injected into the plasma by the e-beam,

[a]Author to whom correspondence should be addressed; Electronic mail: mjk@uiuc.edu
[b]Present address: LAM Research Corp., 4650 Cushing Parkway, Fremont, CA 94538; Electronic mail: wenli.collison@lamrc.com
[c]Electronic mail: druzic@uiuc.edu

Downloaded 23 Dec 2012 to 192.17.144.173. Redistribution subject to AVS license or copyright; see http://avspublications.org/jvsta/about/rights_and_permissions

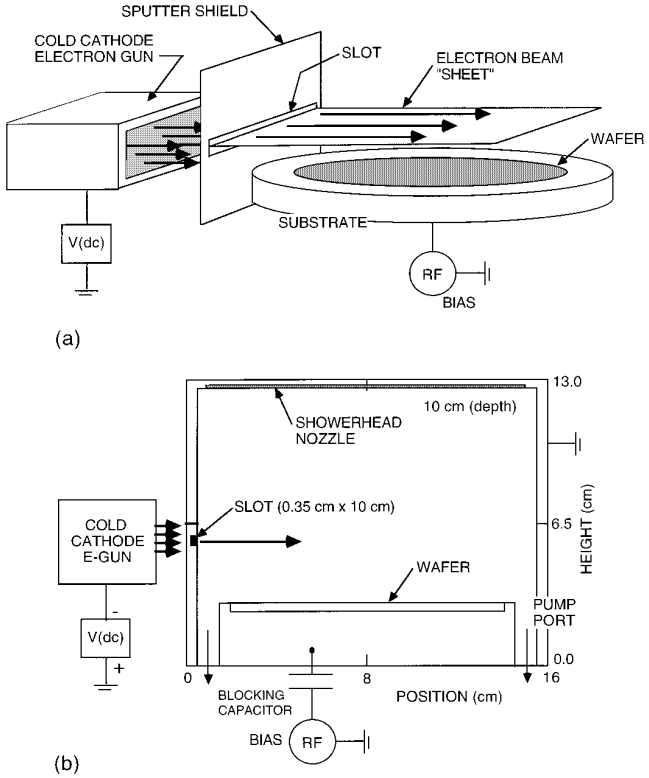

FIG. 1. Schematics of the EBCRF device. (a) Experimental apparatus in which a cold cathode e-beam source produces an electron beam sheet at a preselected height above the substrate. The substrate is independently powered by a rf bias. (b) Geometry used in our model of the EBCRF. In the two-dimensional simulation, the depth was specified as 10 cm.

there must be a dc return current path to ground. This will typically not be the wafer covered biased substrate since the wafer is a dielectric, or a poor conductor, and in any event is capacitively coupled which blocks dc currents. Rather, the current dc current return must be through some other grounded conducting surface in the reactor. The necessity for this dc current path to ground requires special attention when using EBCRF in highly polymerizing etch or deposition systems which coat all surfaces with insulating dielectrics.

In this article, results from a computational study of EBCRF discharges sustained in Ar and Ar/Cl_2 will be presented. The intent of this study is to investigate the parameter space (e-beam voltage, current, and placement) for which the composition, magnitude and energy of the ion flux to the wafer can be separately controlled. The model we have used in this study is described in Sec. II, and results from our parameterization for EBCRF discharges sustained in Ar are discussed in Sec. III. Our study of EBCRF discharges sustained in Ar/Cl_2 is discussed in Sec. IV, followed by our concluding remarks in Sec. V.

II. DESCRIPTION OF THE MODEL

The model employed in this study is based on that described in Refs. 11 and 12, and so the basics of the model will be only briefly discussed. Emphasis will be placed on enhancements and improvements to the previously described model.

The simulation we have used is called the hybrid plasma equipment model (HPEM). The HPEM is a two-dimensional (cylindrical or Cartesian) simulation consisting of three modules; the electromagnetics module (EMM), the electron Monte Carlo simulation (EMCS) and the fluid-kinetics simulation (FKS). The EMM solves for the electric and magnetic fields which are produced by antennas as in ICP reactors. These fields—and electrostatic fields from the FKS—are used in the EMCS where the electron energy distribution is obtained as a function of position. These distributions are used to calculate electron transport coefficients and electron impact source functions which are then passed to the FKS. In the FKS, the densities of all charged and neutral species are solved using continuity and momentum equations, and Poisson's equation is solved for the electric potential. The resulting densities, conductivities and time dependent electric fields are transferred to the EMCS and EMM. This process is iterated until a converged solution is obtained. In this study, antenna generated inductively coupled electric fields are not used, so only the EMCS and FKS modules are employed.

In order to address the electron beam kinetics, we added a module to the HPEM called the electron beam slowing module (EBSM). The EBSM is a Monte Carlo (MC) simulation which uses the same algorithms, cross sections and iterative methodology as the EMCS. The particular implementation we have used is a beam-bulk approach. To begin the EBSM, we specify the location, direction, current density and energy of the electron beam which is injected into the chamber. MC techniques are used to track the flight of the injected electrons and their secondary electron progeny—until they slow below a specified energy—thereby joining the bulk plasma or strike a surface. The details of the implementation of the MC method for e-beam slowing are discussed in Ref. 13. The electrons in the EBSM are advanced in the spatially and time dependent electric field obtained from the FKS in the same fashion as in the EMCS. The electron energy distributions for the injected e-beam and its progeny are calculated as function of position. From those energy distributions, electron impact source functions for all pertinent processes (i.e., dissociation, excitation, ionization) are computed and transferred to the FKS. We also compute the rate of appearance of e-beam electrons as they slow below the energy boundary between the beam and bulk electron distributions. This rate of charge generation (electrons/cm^3 s) is used in the continuity equations in the FKS and constitutes the source of dc current. This source of current is in turn reflected in the electrical potential of the plasma through solution of Poisson's equation. The actual space charge of the beam electrons is not included in solution of Poisson's equation. The density of electrons in the beam is typically $\lesssim 10^7$ cm^{-3} and therefore contributes little to the bulk space charge density.

As an enhancement to the previously described HPEM, we have added momentum equations for all charged (other than electrons) and neutral species to the FKS. The equations

Downloaded 23 Dec 2012 to 192.17.144.173. Redistribution subject to AVS license or copyright; see http://avspublications.org/jvsta/about/rights_and_permissions

we now solve for the density of the ith species n_i are now[14]

$$\frac{\partial n_i}{\partial t} = -\nabla \cdot (n_i \mathbf{v}_i) + S_i + S_e \tag{1a}$$

$$\frac{\partial (n_i \mathbf{v}_i)}{\partial t} = -\frac{\nabla n_i k T_i}{m_i} - \nabla \cdot (n_i \mathbf{v}_i \mathbf{v}_i) + \frac{q_i n_i \mathbf{E}}{m_i} + \sum_j \left(\frac{m_j}{m_i + m_j} \right) n_i n_j \nu_{ij} (\mathbf{v}_j - \mathbf{v}_i), \tag{1b}$$

where $\mathbf{v}_i$ is the velocity of species i, m_i is its molecular weight, q_i is the charge, $\mathbf{E}$ is the electric field and ν_{ij} is the momentum transfer collision frequency between species i and j (neutral–neutral, ion–neutral or ion–ion). S_i is the source function for species i resulting from heavy particle and electron impact (beam and bulk) collisions. S_e is the source of electron current resulting from the slowing of e-beam electrons into the bulk electron distribution. Equation (1) is couched in finite difference form using donor cell algorithms on a staggered mesh. Species densities are solved at cell centers and velocities are at cell boundaries. The inflow and outflow of gas through the reactor are specified as flux boundary conditions for Eq. (1). The surfaces of the chamber which are either input nozzles or pump ports are specified, as well as the input flow of feedstock gases (typically in sccm). Only the feedstock gases are injected at the nozzles; whereas, mole-fraction weighted fluxes of all neutral species are removed at the pump ports. The pumping speed is adjusted to maintain the specified gas pressure.

The electron density is still obtained using drift-diffusion expressions as in Ref. 11. This enables us to retain our implicit solution of Poisson's equation, and therefore take time steps which greatly exceed the dielectric relaxation time.

III. EBCRF DISCHARGES SUSTAINED IN ARGON

The geometry we have employed in this study is shown in Fig. 1(b). The HPEM is a two-dimensional simulation, and in this work we have used Cartesian coordinates. We do not resolve the dimension into the page, and so have specified a depth of 10 cm. The rf biased substrate is 13 cm wide. The grounded reactor walls are separated by 15 cm laterally providing a 1 cm gap on each side of the substrate. The roof of the reactor is 10 cm above the substrate. The e-beam is injected from the left side at a height 2.75 cm above the substrate. The width of the masked sheet of current is ≈0.35 cm. In this section, we will discuss EBCRF discharges sustained in Ar. The species we include in the kinetics are electrons, ground state Ar, Ar* [nominally Ar($4s$)] and Ar^+. The electron impact and heavy particle reactions are the same as discussed in Ref. 11. Unless stated otherwise, the gas pressure is 50 mTorr.

Electron densities for different injected e-beam currents are shown in Fig. 2 for an e-beam voltage of 1500 V. The rf bias is 100 V (amplitude). In the absence of the e-beam, the plasma is uniform across the substrate and has a peak electron density of 8.8×10^{10} cm^{-3}. The beam is injected from the left and has a slowing down length of roughly half the lateral dimension. This produces an ionization source from the e-beam which also extends halfway across the chamber, as shown in Fig. 3(a). The bulk ionization source, Fig. 3(b), is large near the corners of the substrate and chamber due to

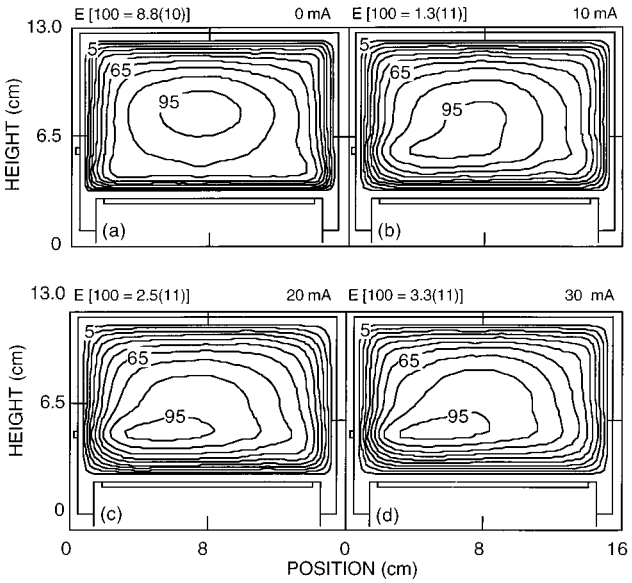

FIG. 2. Electron (or Ar^+) densities (cm^{-3}) for an EBCRF sustained in 50 mTorr of Ar for different e-beam currents. (a) 0 mA, (b) 10 mA, (c) 20 mA, and (d) 30 mA. The e-beam voltage is 1500 V and the rf bias is 100 V (amplitude). The e-beam dominates ionization above a current of ≈10 mA. The contours are labeled with the percentage of the maximum density shown at the top of each figure. 8.8(10) represents 8.8×10^{10} cm^{-3}.

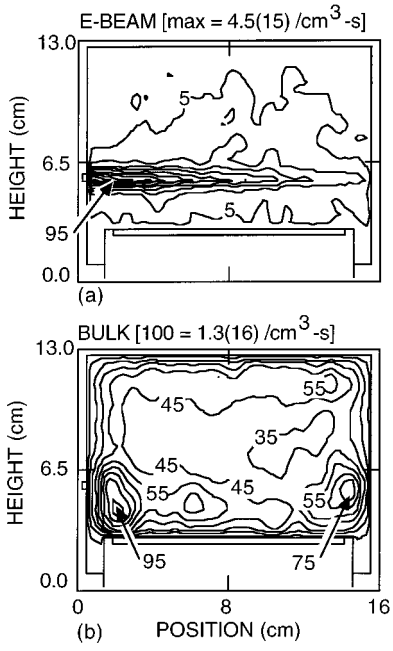

FIG. 3. Ionization sources for Ar^+ from (a) the e-beam and (b) the bulk electrons [V(e-beam)=1500 V, I(e-beam)=60 mA]. The spatial extent of direct ionization by the e-beam is determined by its stopping distance. The contours are labeled with the percentage of the maximum source shown at the top of each figure.

Downloaded 23 Dec 2012 to 192.17.144.173. Redistribution subject to AVS license or copyright; see http://avspublications.org/jvsta/about/rights_and_permissions

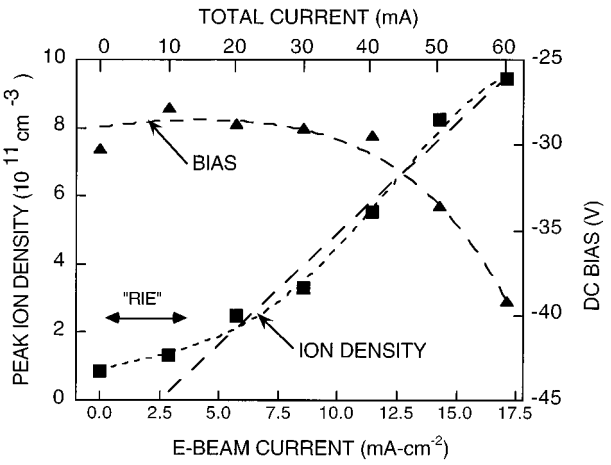

FIG. 4. Peak ion density and dc bias as a function of e-beam current. [Ar, 50 mTorr, V(e-beam)=1500 V, V(bias)=100 V]. Above a threshold e-beam current, the peak ion density increases linearly with beam current. The dc bias is nearly constant over a range of e-beam currents, becoming more negative at large e-beam currents.

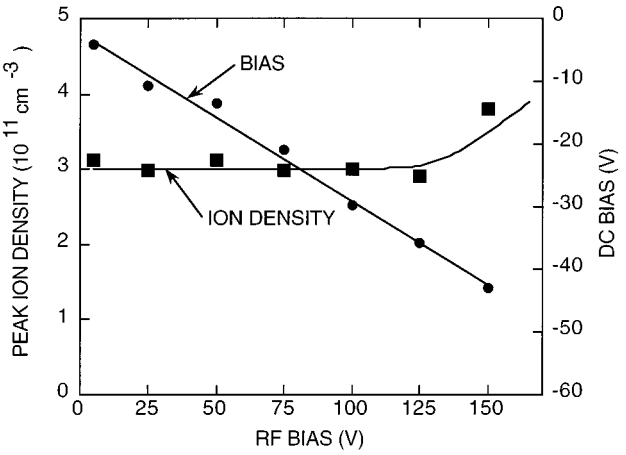

FIG. 5. Peak ion density and dc bias as a function of the amplitude of the rf bias applied to the substrate [Ar, 50 mTorr, V(e-beam)=1500 V, I(e-beam)=40 mA]. Over a wide range of rf biases, the ion density is essentially constant while the dc bias scales linearly with the rf bias. At large rf bias, the thickening sheath produces more electron heating and so more bulk ionization.

either electric field enhancement (outside corners) or the effects of convergent sheaths (inside corners). Note that the peak ionization source from the e-beam is sometimes less than that of the bulk distribution. This result is a bit misleading since the additional ionization provided by the beam also increases the bulk plasma density, thereby, increasing its source function. The generation of secondary electrons in the sheaths by the e-beam also contributes to a bulk ionization source.

As the e-beam current increases, the peak plasma density also increases and becomes asymmetric across the reactor, as shown in Fig. 2. The peak electron density increases to 3.3×10^{11} cm^{-3} for an e-beam current of 8.6 mA/cm^2 (or 30 mA total). The spatial distribution of the electron density is dominated by the e-beam for currents $>3-4$ mA/cm^2 (10–14 mA total). This corresponds to a beam power of 15–20 W, while the bias power is 15 W. Although the rf bias voltage is constant (100 V), the rf bias power increases as the e-beam current (and ion density) increases. For example, the rf bias power increases from 12 W with no e-beam current to 37 W at 60 mA of e-beam current. This increase in rf bias power results from the larger ion flux generated by the e-beam which is then accelerated by the fixed rf bias into the substrate.

The peak ion density and dc bias on the substrate are shown in Fig. 4 as a function of e-beam current. The rf bias is constant at 100 V (amplitude) and the e-beam voltage is 1500 V. At low e-beam currents (<4 mA/cm^2, 14 mA total), the ion density is nearly constant. At these low e-beam currents the discharge operates as a conventional RIE discharge. As the e-beam current increases, the ion density becomes nearly linearly proportional to the e-beam current and hence e-beam power. These results indicate that above a threshold e-beam current (≈4 mA/cm^2 in this example) the ion density, and hence ion flux, to the substrate can be controlled by the e-beam power. The dc bias remains essentially constant at -32 V until the e-beam current exceeds ≈10 mA/cm^2 (35 mA total). Above this value the dc bias becomes somewhat more negative. These results indicate that the ion energy to the substrate will not significantly change as the ion flux is varied by changing the e-beam current. This trend agrees with previously reported experimental observations.[10]

Over the range of e-beam currents investigated, the power efficiency of ion production based on total power deposition (e-beam plus rf bias) improves only from 3.6×10^9/cm^3 W without e-beam current to 3.8×10^9/cm^3 W with 60 mA of e-beam current. Even though the efficiency for ionization is higher for e-beam electrons than for bulk electrons, the additional power dissipation by the rf bias due to ion acceleration tends to lower the total ionization efficiency at high e-beam currents.

The peak ion density and dc bias as a function of amplitude of the rf bias are shown in Fig. 5 for an e-beam energy of 1500 V and an e-beam current of 11.5 mA/cm^2 (40 mA total, 60 W). For an rf bias of $\leqslant125$ V, the ion density is essentially constant while the dc bias increases (becomes more negative) in proportion to the rf bias. The fact that the ion density does not increase with increasing rf bias is partly a result of operating at a high e-beam generated plasma density which produces a thin sheath. Since stochastic heating of electrons is proportional to the sheath velocity—which scales as sheath thickness $\times$ rf frequency—there is little electron heating produced by the rf bias. It is only at the higher rf bias which produces a thicker sheath—and hence higher sheath velocity—that sufficient stochastic electron heating occurs to increase the ion density. The results of Figs. 4 and 5 demonstrate that for a fixed rf bias, the ion density and flux to the substrate can be controlled by the e-beam current while not affecting the dc bias. Analogously for a fixed e-beam current, the ion flux is constant while the rf (and dc) bias increase. That is, ion flux and ion energy can be independently controlled.

Downloaded 23 Dec 2012 to 192.17.144.173. Redistribution subject to AVS license or copyright; see http://avspublications.org/jvsta/about/rights_and_permissions

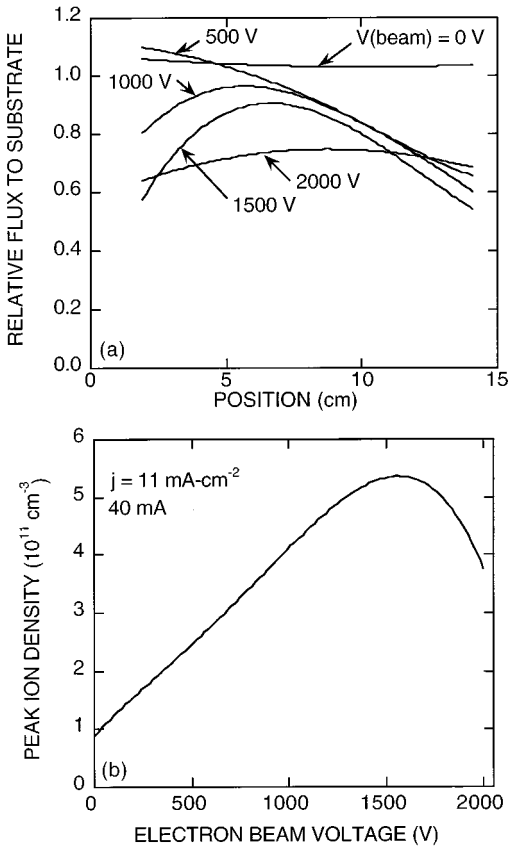

FIG. 6. EBCRF characteristics for different e-beam voltages [Ar, 50 mTorr, I(e-beam)=40 mA, V(bias)=100 V]. (a) Ion flux to the substrate as a function of position and (b) peak ion density. (The ion fluxes have been renormalized so that their spatial distributions can be more readily compared.) Since the e-beam stopping distance increases with increasing voltage, the uniformity of the ion flux to the substrate generated by the e-beam improves with higher voltages. This improvement may come at the expense of ion density since an e-beam which penetrates far through the gas is not producing significant ionization.

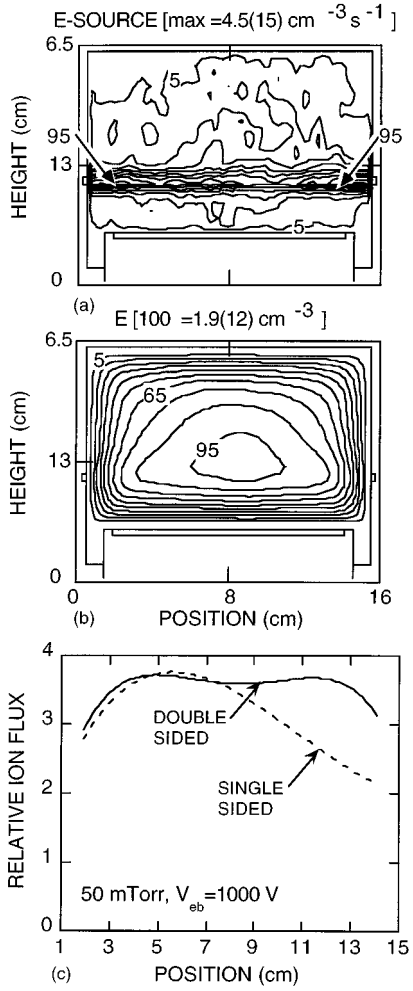

FIG. 7. EBCRF characteristics for double sided e-beam pumping [Ar, 50 mTorr, V(e-beam)=1000 V, I(e-beam)=60 mA total for both beams, V(bias) =100 V]. (a) Ionization source by the e-beams, (b) electron (or Ar^+) density, and (c) ion flux to the substrate. The overlapping of the slowing down regions of the opposing e-beams produces a uniform ionization source and ion density. The result is a uniform ion flux to the substrate compared to the single sided case. The contours are labeled with the percentage of the maximum density or source shown at the top of each figure.

In material processing the uniformity of the ion flux across the substrate is an important consideration. The ion densities shown in Fig. 2 produce a nonuniform ion flux to the substrate since the stopping distance of the beam is shorter than the width of the substrate. The etch rate for ion driven processes may then also be nonuniform. For example, the Si etch rate produced in the EBCRF discharge reported in Ref. 10 monotonically decreased across the substrate from the e-beam injection point. The etch rate directly correlated with power deposition by the e-beam and its slowing profile. Obtaining uniform etching in an EBCRF is therefore largely determined by having uniform power deposition by the e-beam. The stopping distance of the e-beam is proportional to V/P (e-beam voltage/gas pressure). In the high energy limit, inelastic electron impact cross sections scale as $1/\epsilon$, so higher energy e-beams penetrate further through the gas. For a constant e-beam voltage lower gas pressures produce lower collision rates which also produce a longer stopping length.

This scaling is shown in Fig. 6(a) where ion fluxes to the substrate are plotted as a function of e-beam voltage (e-beam current=11.4 mA/cm^2, 40 mA total). In the absence of the e-beam, the ion flux is nearly uniform across the substrate. With a low voltage e-beam, the stopping distance is short, so the ion flux is highest near the e-beam injection point. As the e-beam voltage increases, the stopping distance lengthens and the ion flux to the substrate becomes more uniform. At an e-beam energy of 2000 V, the ion flux has regained a uniform distribution. Unfortunately this improvement in uniformity is accomplished at the expense of ionization efficiency since an e-beam which has a long stopping distance does not experience many depleting ionizing collisions. That is, it is difficult to achieve both uniform *and* efficient e-beam pumping with a single beam. For example, the peak ion density as a function of e-beam voltage is shown in Fig. 6(b). Although the large e-beam voltages generate more uniform ion fluxes, the peak ion density is also lower.

This trade off between uniformity and pump rate is a well known problem in e-beam pumping of high pressure (>1

Downloaded 23 Dec 2012 to 192.17.144.173. Redistribution subject to AVS license or copyright; see http://avspublications.org/jvsta/about/rights_and_permissions

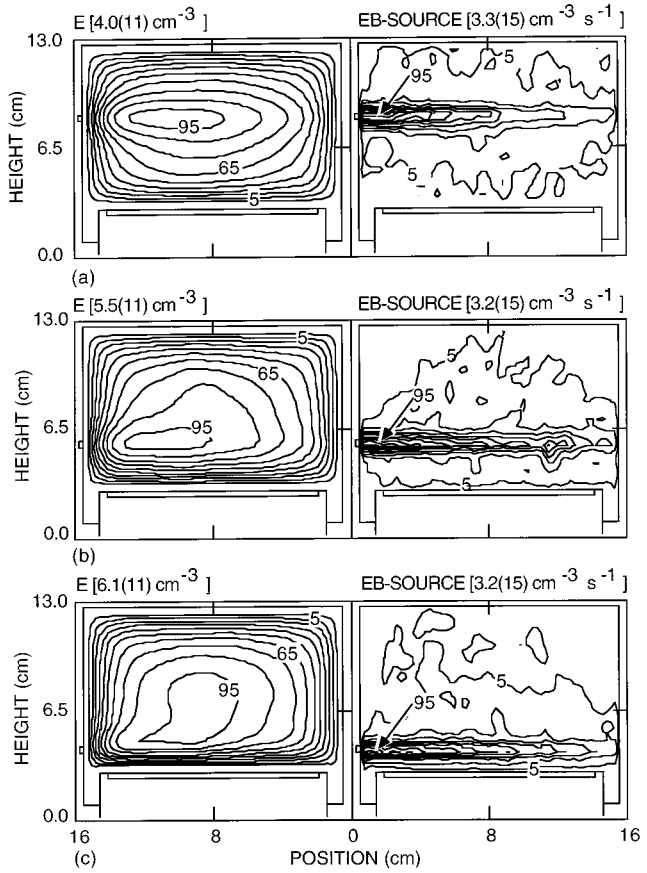

FIG. 8. Electron (or Ar^+) density and ionization source by the e-beam for different heights of the e-beam above the substrate [Ar, 50 mTorr, V(e-beam) =1500 V, I(e-beam)=40 mA, V(bias)=100 V]. (a) 5.5 cm, (b) 2.7 cm, and (c) 1.7 cm. The peak ion density increases as the e-beam approaches the substrate, possibly due to production of secondary electrons in high field regions. The contours are labeled with the percentage of the maximum density or source shown at the top of each figure.

atm) gas lasers.[15] The quandary has been partially remedied by using double sided e-beam pumping where the sum of two nonuniform pump profile resulting from the opposing e-beams produces a fairly uniform excitation source. This strategy is demonstrated in Fig. 7 where the e-beam ionization rates, ion density and ion flux to the substrate are shown when we excite the gas with two opposing e-beams of 1000 V. The e-beam ionization source above the substrate is essentially uniform, which in turn generates a uniform ion density. The uniformity of the ion flux to the wafer is significantly improved over single sided pumping.

Another variable in determining the uniformity of the ion flux is the height of the injected beam above the substrate. The e-beam ionization source and plasma density are shown in Fig. 8 for three heights of the e-beam [1500 V, 11.5 mA/cm^2 (40 mA total)] above the substrate. The ion flux to the substrate for these cases is shown in Fig. 9. The magnitude of the e-beam ionization source is essentially constant as a function of height although the peak ion density increases as the beam approaches the substrate. This trend may be due to e-beam ionization occurring in the sheaths which produces energetic secondary electrons by sheath acceleration. When the e-beam is close to the substrate, the ion flux to the substrate mirrors the e-beam stopping profile and is not uniform. As the e-beam is raised higher above the substrate, the ion density and ion flux appears more diffusional and more uniform.

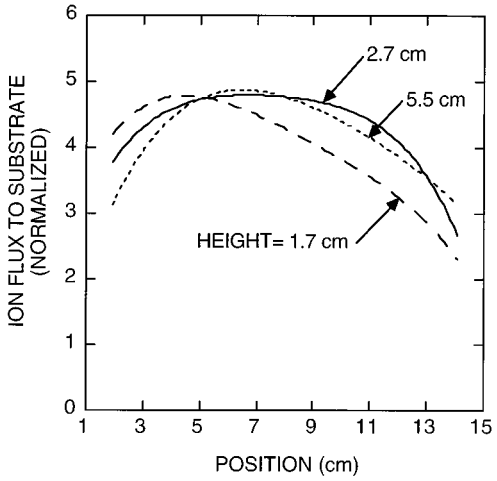

FIG. 9. Ion flux to the substrate as a function of position for different heights of the e-beam above the substrate [Ar, 50 mTorr, V(e-beam)=1500 V, I(e-beam)=40 mA, V(bias)=100 V]. (The ion fluxes have been normalized to enable a more direct comparison.) The ion flux is less uniform, and more closely resembles the ionization source, when the e-beam is located close to the substrate.

IV. EBCRF DISCHARGES SUSTAINED IN Ar/Cl_2

Parameterizations were performed of EBCRF discharges sustained in Ar/Cl_2=70/30 gas mixtures while etching a polysilicon substrate. Gas is injected from the shower head nozzle at the rate of 100 sccm [see Fig. 1(b)]. The reaction chemistry is the same as in Ref. 12 with the exception that $SiCl_2$ is specified as being the etch product. The important additional reactions we included are electron impact dissociation[16] and ionization of $SiCl_2$ and SiCl.

Typical results from the model for the charged particle densities in the Ar/Cl_2 EBCRF discharge (35 mTorr, V_{rf}=100 V, V_{eb}=1500 V, I_{eb}=40 mA) are shown in Fig. 10. In this reaction chemistry, Ar^+ has the highest ionization potential. It is dominantly produced by electron impact ionization by e-beam electrons, and is rapidly depleted by charge exchange to Cl_2 producing Cl_2^+ and Cl^+. Cl^+ is also produced by direct electron impact on Cl atoms. The Cl^+ ion can then charge exchange with Cl_2 to produce Cl_2^+. The end result is the spatial extents of Ar^+ and Cl^+ are largely defined by the slowing down length of the e-beam. Cl_2^+, which is the end product of the charge exchange chain, has a more uniformly spatially distributed density. The Cl^- density peaks within the slowing down zone of the e-beam. Since this is the region of the highest production of positive ions the plasma potential is, on a time averaged basis, most positive there. The cool negative ions therefore pool to their maximum density in the e-beam slowing region. $SiCl^+$ and $SiCl_2^+$ ions are

Downloaded 23 Dec 2012 to 192.17.144.173. Redistribution subject to AVS license or copyright; see http://avspublications.org/jvsta/about/rights_and_permissions

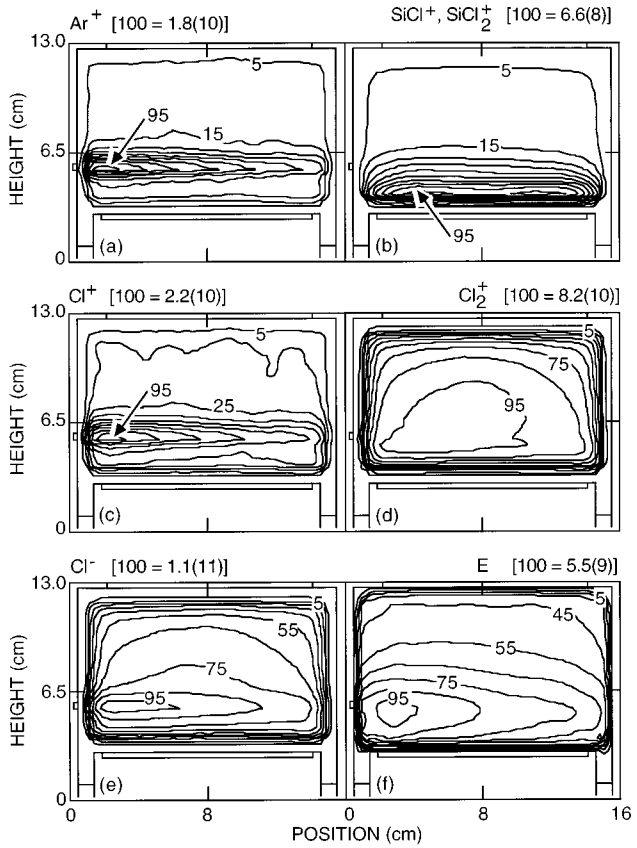

FIG. 10. Charged particle densities in an EBCRF sustained in an Ar/Cl_2=70/30 gas mixture at 35 mTorr [V(e-beam)=1500 V, I(e-beam)=40 mA, V(bias)=100 V]. (a) Ar^+, (b) $SiCl^+$ and $SiCl_2^+$, (c) Cl^+, (d) Cl_2^+, (e) Cl^-, and (f) electrons. Ions having high ionization potentials, such as Ar^+, which charge exchange to other species have densities which mirror the e-beam ionization source. The contours are labeled with the percentage of the maximum density shown at the top of each figure.

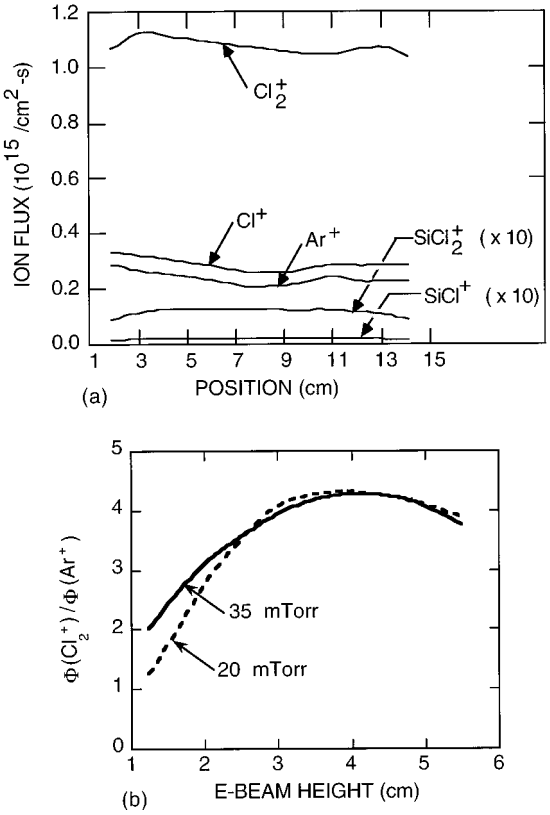

FIG. 11. Ion fluxes to the substrate for the Ar/Cl_2 gas mixture. (a) Fluxes for all ions as a function of position. (b) Ratio of the Cl_2^+ ion flux to the Ar^+ ion flux as a function of the height of the e-beam above the substrate. The ion flux is depleted of Ar^+ when the e-beam and ionization source is far from the substrate.

most plentiful near the substrate where the $SiCl_2$ etch product is generated.

The scaling laws discussed for Ar EBCRF discharges in the previous section generally hold for the more complex gas mixture. The exception is that independent control of the flux and energy of ions incident onto the substrate is typically not achieved until higher power deposition by the e-beam than is required in Ar discharges. This scaling can be expected to be a general result for highly attaching gas mixtures, such as Ar/Cl_2. Obtaining independent control of ion flux and ion energy requires that the rf bias power contribute little to electron heating and ionization. This is typically achieved by having a thin sheath which in turn requires a high electron density. The electron density is usually lower in attaching gas mixtures for a given power deposition. Therefore for otherwise similar conditions, independent control of the ion flux and energy requires higher power deposition by the e-beam to broach the thin sheath limit in attaching gas mixtures.

Another possible feature of the EBCRF discharge is the ability to control the composition of the ion flux to the substrate as well as its magnitude. This control results from choosing the site at which ions are dominantly generated by varying the height of the e-beam above the substrate. By doing so charge exchange reactions filter the ion flux generated by the e-beam by depleting the flux of high ionization potential species prior to reaching the substrate. In the introduction, we discussed the case where Ar^+ ions generated by the e-beam can be filtered from the ion flux which reaches the substrate. This is accomplished by positioning the e-beam at a sufficient height above the substrate that charge exchange reactions with Cl_2 deplete the Ar^+ ions. This ability to filter the ion flux is demonstrated in Fig. 11. Here we show ion fluxes to the substrate for an EBCRF discharge in Ar/Cl_2=70/30 (35 mTorr) for conditions where Ar ionization is dominated by the e-beam. Ion fluxes for all species are shown in Fig. 11(a) for an e-beam height above the substrate of 2.7 cm. The ratio of the Ar^+ flux to Cl_2^+ flux to the substrate is shown in Fig. 11(b) as a function of e-beam height. When the e-beam is close to the substrate at low pressures, the Ar^+ flux is comparable to the Cl_2^+ flux. As the e-beam is raised above the substrate—thereby also raising the Ar^+ ionization source—the flux of Ar^+ is depleted relative to Cl_2^+. The longer path length from the site of e-beam ionization to the substrate results in more charge exchange collisions which convert Ar^+ to Cl_2^+.

Downloaded 23 Dec 2012 to 192.17.144.173. Redistribution subject to AVS license or copyright; see http://avspublications.org/jvsta/about/rights_and_permissions

V. CONCLUDING REMARKS

A parametric computational study of an electron beam controlled rf discharge has been presented. We have demonstrated that in carefully designed EBCRF discharges, the magnitude of the ion flux to the substrate can be controlled by the e-beam power, while the energy of the ion flux to the substrate is controlled by the rf bias. At large rf biases, independent control of the ion flux is compromised by stochastic electron heating which may occur as a result of a thickening sheath. The uniformity of the ion flux is largely determined by the stopping distance of the e-beam which is, in turn, proportional to V/P. Higher e-beam voltages and lower pressures produce more uniform ion fluxes at the expense of ionization efficiency. This efficiency may be recouped by employing doubled sided e-beam pumping. Independent control of ion fluxes and energies generally requires higher power deposition in attaching gas mixtures due to the necessity to produce a thin sheath which requires a critically large electron density. Moderate control of the composition of the ion flux can be achieved by positioning the e-beam at an appropriate height above the substrate and allowing charge exchange collisions to filter the ion flux.

ACKNOWLEDGMENTS

This work was supported by the National Science Foundation (DMR 92-01689, ECS 94-04133), the Semiconductor Research Corporation, and the University of Wisconsin ERC for Plasma Aided Manufacturing.

[1]*Plasma Etching: An Introduction*, edited by D. M. Manos and D. L. Flamm (Academic, Boston, 1989).
[2]J. Asmussen in *Handbook of Plasma Processing Technology*, edited by S. M. Rossnagel, J. J. Cuomo, and W. D. Westwood (Noyes, Park Ridge, NJ, 1990), Chap. 11.
[3]W. M. Holber and J. Forster, J. Vac. Sci. Technol. A **8**, 3720 (1990).
[4]K. Kirmse, A. E. Wendt, G. S. Orhrlein, and Y. Zhang, J. Vac. Sci. Technol. A **12**, 1287 (1994).
[5]J. Hopwood, Plasma Sources Sci. Technol. **1**, 109 (1992).
[6]J. H. Keller, J. C. Forster, and M. S. Barnes, J. Vac. Sci. Technol. A **11**, 2487 (1993).
[7]M. S. Barnes, J. C. Forster, and J. H. Keller, Appl. Phys. Lett. **62**, 2622 (1993).
[8]R. Patrick, R. Schoenborn, and H. Toda, J. Vac. Sci. Technol. A **11**, 1296 (1993).
[9]J. B. Carter, J. P. Holland, E. Peltzer, B. Richardson, E. Bogle, H. T. Nguyen, Y. Melaku, D. Gates, and M. Ben-Dor, J. Vac. Sci. Technol. B **11**, 1301 (1993).
[10]K. D. Schatz and D. N. Ruzic, Plasma Sources Sci. Technol. **2**, 100 (1993).
[11]P. L. G. Ventzek, M. Grapperhaus, and M. J. Kushner, J. Vac. Sci. Technol. B **12**, 1 (1994).
[12]R. J. Hoekstra and M. J. Kushner, J. Appl. Phys. **77**, 3668 (1995).
[13]M. J. Kushner, J. Appl. Phys. **66**, 2297 (1989).
[14]W. Z. Collison and M. J. Kushner, Appl. Phys. Lett. (submitted).
[15]L. A. Rosocha, J. A. Hanlon, J. McLeod, M. Kang, B. L. Kortegaard, M. D. Burrows, and P. S. Bowling, Fusion Technol. **11**, 497 (1987).
[16]Cross sections for these processes were obtained from V. McKoy (private communication, 1995).

Downloaded 23 Dec 2012 to 192.17.144.173. Redistribution subject to AVS license or copyright; see http://avspublications.org/jvsta/about/rights_and_permissions